RSC Advances

Styryl phenanthrimidazole-fluorescence switched on by core/shell BaTiO3/ZnO and Mn-doped TiO2/ZnO nanospheres and switched off by the core nanoparticles

Journal:	*RSC Advances*
Manuscript ID:	RA-ART-09-2014-010303.R1
Article Type:	Paper
Date Submitted by the Author:	11-Oct-2014
Complete List of Authors:	Jayabharathi, Jayaraman; Annamalai University, Chemistry Karunakaran, C. ; Annamalai University, Chemistry Arunpandiyan, Anandan; Annamalai university, chemistry Vinayagamoorthy, Pazhamalai; Annamalai University, Chemistry

Graphical abstract

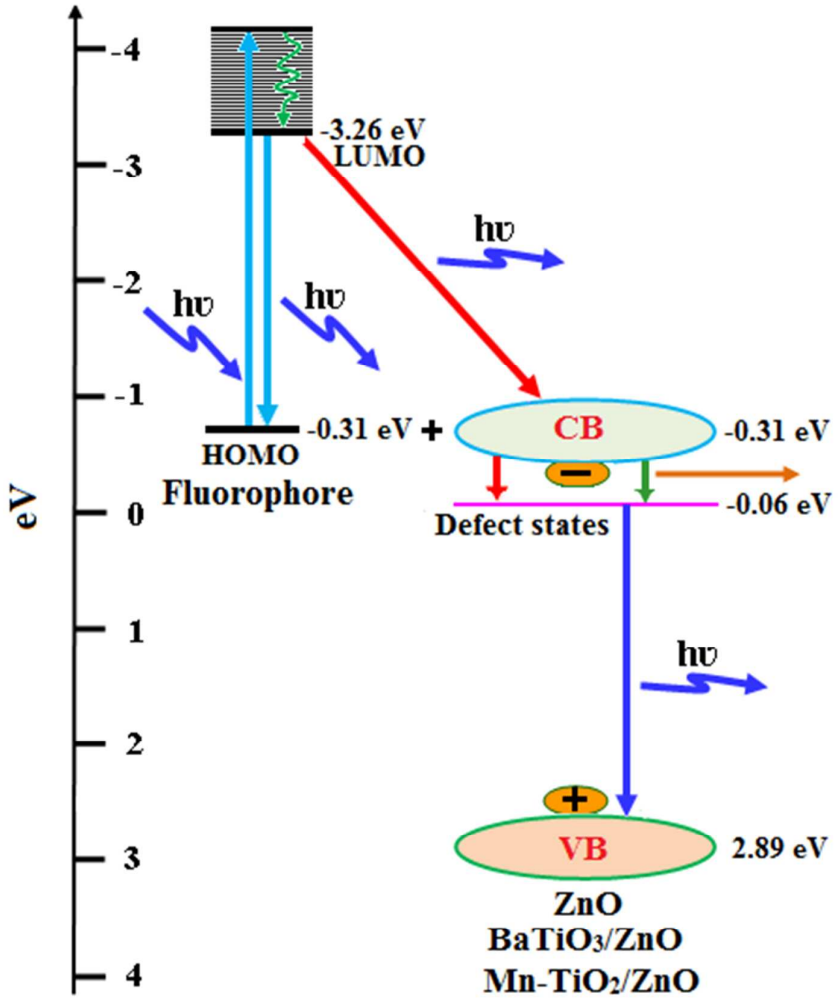

(E)-1-phenyl-2-styryl-1H-phenanthro[9,10-d]imidazoles (PSPI) adsorbed on ZnO (or) Mn-TiO_2/ZnO (or) $BaTiO_3$/ZnO

Styryl phenanthrimidazole-fluorescence switched on by core/shell $BaTiO_3$/ZnO and Mn-doped TiO_2/ZnO nanospheres and switched off by the core nanoparticles

J. Jayabharathi*, C. Karunakaran, A. Arunpandiyan, P. Vinayagamoorthy

Department of Chemistry, Annamalai University, Annamalainagar 608 002, Tamilnadu, India.

*Address for correspondence
Dr. J. Jayabharathi
Professor of Chemistry
Department of Chemistry
Annamalai University
Annamalainagar 608 002
Tamilnadu, India.
Tel: +91 9443940735
E-mail: jtchalam2005@yahoo.co.in

* Corresponding author. Tel.: +91 9443940735
E-mail address: jtchalam2005@yahoo.co.in

Styryl phenanthrimidazole-fluorescence switched on by core/shell $BaTiO_3$/ZnO and Mn-doped TiO_2/ZnO nanospheres and switched off by the core nanoparticles

J. Jayabharathi*, C. Karunakaran, A. Arunpandiyan, P. Vinayagamoorthy

Department of Chemistry, Annamalai University, Annamalainagar 608 002, Tamilnadu, India.

Abstract

Absorption, fluorescence and lifetime spectral studies have been made to probe the interaction of fluorophore (E)-1-phenyl-2-styryl-1H-phenanthro[9,10-d]imidazole with sol-gel synthesised $BaTiO_3$/ZnO and Mn-doped TiO_2/ZnO core/shell and pristine ZnO nanospheres and $BaTiO_3$ and Mn-doped TiO_2 nanoparticles. The emission of fluorophore is switched on by Mn-doped TiO_2/ZnO and $BaTiO_3$/ZnO core/shell and pristine ZnO nanospheres and switched off by Mn-doped TiO_2 and $BaTiO_3$ nanoparticles owing to charge injection from the excited singlet state of fluorophore to the conduction band (CB) of the nanosemiconductors. The affinity of the fluorophore to ZnO results in lowering HOMO and LUMO energy levels of fluorophore leading to emission at ~420 nm. This is due to LUMO → HOMO, LUMO → CB and deep level emission (DLE) of ZnO resulting in enhancement of fluorescence. The HOMO and LUMO energy levels of the fluorophore are unlikely to be influence by core $BaTiO_3$ and Mn –doped TiO_2 nanoparticles. This leads to quenching of fluorescence because of electron transfer from LUMO → CB.

Keywords: Mn-doped TiO_2/ZnO; $BaTiO_3$/ZnO; Enhancement; Quenching; Charge injection.

* Corresponding author. Tel.: +91 9443940735
E-mail address: jtchalam2005@yahoo.co.in

1. Introduction

ZnO nanostructures with a band gap of *ca*. 3.2 eV and an exciton binding energy of 60 meV have exponential applications in nanoelectronics [1], nanooptelectronics [2], nanopiezotronics [3], varistor devices [4], field emission devices [5], thin-film transistors [6], lasers [7], dye-sensitized solar cells (DSSC) [8], gas sensors [9], sunscreens [10], catalysis [11], photocatalysis [12] and bacteria disinfection [13]. Investigation of light induced electron transfer from N-containing heterocyclic molecules to nanostructured semiconductor is of interest due to its pivotal role in DSCC [14], medicine for diagnostics and imaging [15] and photodynamic therapy [16]. Since nanocrystals possess large surface to volume ratio, wherein the surface ions are under-coordinated compared to the coordination number at the core of the nanocrystals. The under-coordinated surface sites can be passivated with organic molecules by stabilizing the nanocrystals. Optical properties of semiconductor nanocrystals are affected by the nanocrystal -organic molecule interface [17–19]. Photogenerated electron–hole pairs can recombine radiatively or non-radiatively depending upon the energy levels of the nanocrystal-organic molecule interface and thereby influence the luminescence efficiency [18]. A red-shift absorption was observed when phenyldithiocarbamate binds to the CdSe nanocrystal surface since the HOMO of the molecule has the appropriate energy and symmetry to interact with the valence states of the nanocrystal [18]. Charge-transfer process the semiconductor nanocrystal-organic molecule interface plays a vital role and affects the optical properties of the nanocrystals. Study of charge-transfer process is of importance since the luminescence of nanocrystals find useful applications in biology and optoelectronic devices.

As far as we know, most of the studies reported so far are on the effect of ligands on the optical properties of nanocrystals [20] and there is no such study with core/shell nanospheres.

Herein we report the electron transfer from photoexcited fluorophore to ZnO shell of Mn-doped TiO_2/ZnO and $BaTiO_3$/ZnO core/shell nanospheres as well as to Mn-doped TiO_2 and $BaTiO_3$ nanoparticles. The Mn-doped TiO_2/ZnO and $BaTiO_3$/ZnO core/shell nanospheres, like ZnO nanospheres, switched on the emission of fluorophore moiety. The observed fluorescence enhancement throws light on the interaction between the fluorophore and nanomaterials i.e., know the electron transfer from the bioactive fluorophore molecule to semiconductor core/shell nanospheres. The fluorescence emission is switched off by Mn-doped TiO_2 and $BaTiO_3$ nanoparticles owing to charge injection from the excited singlet state of the fluorophore to the conduction band (CB) of the TiO_2 nanoparticles.

2. Materials and methods

2.1. Materials and measurements

Phenanthroquinone, cinnamaldehyde and all other reagents have been purchased from Sigma-Aldrich. The ultraviolet-visible (UV-vis) spectra were obtained with Perkin Elmer Lambda 35 UV-vis spectrophotometer and corrected for background absorption due to solvent. Photoluminescence (PL) spectra were recorded on a PerkinElmer LS55 fluorescence spectrometer. NMR spectra were recorded on Bruker 400 MHz NMR spectrometer. The mass spectra of the samples were obtained using an Agilent LCMS VL SD in electron ionization mode. Cyclic voltammetry (CV) analyses were performed by using CHI 630A potentiostat electrochemical analyzer. Fluorescence lifetime measurements were carried out with a nanosecond time correlated single photon counting (TCSPC) spectrometer Horiba Fluorocube-01-NL lifetime system with Nano LED (pulsed diode excitation source) as the excitation source and TBX-PS as detector. The absolute quantum yields were measured by comparing fluorescence intensities (integrated areas) of a standard sample. Theoretical calculations were

performed using density functional theory (DFT) as implemented with Gaussian-03 program using the Becke3-Lee-Yang-Parr (B3LYP) functional supplemented with the standard 6-31G (d, p) basis set [21].

Methanolic solution of the fluorophore of required concentration was mixed with the nanoparticles dispersed in methanol at different loading and the absorption (10 μM) and emission (0.1 nM) spectra were recorded. The Mn-doped TiO_2 and $BaTiO_3$ nanoparticles, $BaTiO_3$/ZnO and Mn-doped TiO_2/ZnO core/shell nanospheres and pristine ZnO nanospheres were dispersed under sonication in methanol.

2.2. Synthesis of (E)-1-phenyl-2-styryl-1H-phenanthro[9,10-d]imidazole (fluorophore)

A mixture of phenanthriquinone (1 mmol), cinnamaldehyde (1 mmol), aniline (1 mmol), ammonium acetate (1mmol) and indium trifluoride (InF_3, 1 mol %) was stirred at 80 °C. The progress of the reaction was monitored by TLC. After completion of the reaction, the mixture was cooled, dissolved in acetone and filtered. The product was purified by column chromatography using benzene: ethyl acetate (9:1) as the eluent [22]. M.p. 208 ºC; Anal. calcd. for $C_{29}H_{20}N_2$: C 87.85, H 5.08, N 7.07; Found. C 87.81, H 5.02, N 7.03; ^{1}H NMR (400 MHz, DMSO) δ: 6.69 (d, J = 16 Hz, 1H), 7.07 (d, J = 7.6 Hz, 1H), 7.33-7.36 (m, 6H), 7.48-7.54 (m, 3H), 7.68-7.87 (m, 8H), 8.20 (d, J = 7.6Hz, 1H), 8.87 (q, J = 8Hz, 2H); ^{13}C NMR (100 MHz, DMSO): δ: 113.82, 120.17, 122.12, 123.65, 124.46, 125.21, 125.81, 126.46, 126.66, 126.84, 127.82, 127.42, 127.79, 128.29, 128.32, 128.66, 128.79, 128.92, 130.38, 130.53, 134.38, 135.69, 136.73, 136.93, 149.24; MS: m/z 396 [M^+].

2.3. Core/shell $BaTiO_3$/ZnO and Mn-doped TiO_2/ZnO nanospheres

Core/shell $BaTiO_3$/ZnO and Mn-doped TiO_2/ZnO nanoparticles were synthesized by sol-gel method using polyethylene glycol 20,000 as template and characterized by high resolution

scanning electron microscopy (HR-SEM), powder X-ray diffractometry (XRD), and energy dispersive X-ray (EDX), solid state impedance, UV-visible diffuse reflectance and photoluminescene spectroscopies [23].

3. Results and discussion

3.1. Absorption characteristics of fluorophore – core/shell $BaTiO_3$/ZnO and Mn-TiO_2/ZnO and pristine ZnO nanospheres and Mn-TiO_2 and $BaTiO_3$ nanoparticles

Figure 1 presents the HR-SEM images of core/shell $BaTiO_3$/ZnO and Mn-doped TiO_2/ZnO nanospheres. They display the spherical shape of the synthesized nanoparticles. Due to Ostwalds ripening some deformation of the shape is observed. However most of the particles are spherical in shape and the synthesised samples are named as nanospheres [24]. The absorption spectra of fluorophore in the presence of $BaTiO_3$/ZnO and Mn-doped TiO_2/ZnO core/shell and pristine ZnO nanospheres and Mn-doped TiO_2 and $BaTiO_3$ nanoparticles dispersed at different loading and also in their absence are displayed in Figure 2. The nanoparticles enhance the absorbance of fluorophore remarkably without shifting its absorption maximum. This indicates that core/shell $BaTiO_3$/ZnO and Mn-doped TiO_2/ZnO nanospheres, pristine ZnO nanospheres and Mn-doped TiO_2 and $BATiO_3$ nanoparticles do not modify the excitation process of the fluorophore molecule. The enhanced absorbance observed with the dispersed nanoparticles is due to adsorption of fluorophore on the surfaces of core/shell $BaTiO_3$/ZnO and Mn-doped TiO_2/ZnO and pristine ZnO nanospheres and Mn-doped TiO_2 and $BaTiO_3$ nanoparticles. This is because of electron transfer from the excited state of the fluorophore to the conduction band (CB) of the semiconductor nanoparticles [25].

3.2. Fluorescence switched on by $BaTiO_3$/ZnO and Mn-doped TiO_2/ZnO core/shell and pristine ZnO nanospheres

The emission spectra of fluorophore in presence of $BaTiO_3$/ZnO and Mn-doped TiO_2/ZnO core/shell and pristine ZnO nanospheres dispersed at different loading and also in their absence are displayed in Figure 3. The $BaTiO_3$/ZnO and Mn-doped TiO_2/ZnO core/shell and pristine ZnO nanospheres switched on the emission of fluorophore remarkably without shifting its emission maximum at 421 nm. This indicates that the nanoparticles do not modify the excitation process of the fluorophore. The enhanced emission observed with the dispersed nanospheres is due to adsorption of the fluorophore on ZnO surface. The emission enhancement due to effective transfer of electron from the excited state of the fluorophore to the CB of ZnO shell of $BaTiO_3$/ZnO and Mn-doped TiO_2/ZnO core/shell and pristine ZnO nanospheres.

Fluorescence enhancement arises due to the formation of fluorophore – ZnO and fluorophore – $BaTiO_3$/ZnO and fluorophore – Mn-doped TiO_2/ZnO core/shell nanosphere complexes. Figure 4 shows the Stern -Volmer plot [26] of fluorophore with various loadings of ZnO, $BaTiO_3$/ZnO and Mn-doped TiO_2/ZnO core/shell nanospheres. The binding constant for Mn-doped TiO_2/ZnO, $BaTiO_3$/ZnO core/shell and pristine ZnO nanospheres are 2.0 x 10^7 M^{-2}, 2.0 x 10^7 M^{-2} and 2.6 x 10^7 M^{-2}, respectively. The binding constant shows that the ligand is strongly bound to the ZnO nanospheres than to core/shell Mn-dopedTiO_2/ZnO and $BaTiO_3$/ZnO nanospheres. The binding of the ligand in the core/shell nanosphere is through the ZnO shell of the core/shell nanospheres. The number of biding site (n) have been deduced using the equation [27], log $[F_0 - F /F]$ = log K + nlog[nanoparticles] as two; *i.e.*, each fluorophore molecule is bound to two ZnO, probably each nitrogen is attached to one ZnO through Zn^{2+}.

3.3. Enhancement mechanism

From the onset oxidation potential (E_{ox}) and the onset reduction potential (E_{red}) of the fluorophore, the HOMO and LUMO energy levels have been calculated using the formulae HOMO = $-e(E_{ox} + 4.71)$ (eV) and LUMO = $-e(E_{red} + 4.71)$ (eV). The energy levels of fluorophore molecule and the semiconductors show that electron injection is thermodynamically allowed from the excited singlet of the fluorophore to the CB of pristine ZnO, ZnO shell of Mn-doped TiO_2/ZnO and $BaTiO_3$/ZnO nanospheres. Figure 5 presents the HOMO and LUMO energy levels of fluorophore and the CB and valence band (VB) edges of ZnO and core/shell Mn-doped TiO_2/ZnO and $BaTiO_3$/ZnO nanospheres. The electron in the LUMO of the excited molecule is of higher energy than that in the CB of the semiconductors. This should lead to transfer of electron from LUMO of the excited molecule to the CB of ZnO. The excess energy (~2.95 eV) is released in the form of light and the wavelength of emission radiation corresponding to the excess energy is 420 nm. This additional path of emission opened, besides the LUMO→HOMO (fluorophore) and deep level emission (DLE), accounts for the enhancement of fluorescence. That is, on irradiation at 250 nm both fluorophore and ZnO are excited. Duel emission is expected due to LUMO→HOMO and DLE transition; ZnO exhibits emission at ~420 nm because of band edge free excitons [28] and the excited fluorophore emits fluorescence at 421 nm. Also possible is electron jump from the excited fluorophore to the nanosphere. Generally the electron transfer injection from the LUMO of the fluorophore to the CB of semiconductor is to quench the fluorophore. However in the present cases the HOMO energy level of the fluorophore matches with that of the CB of ZnO and this accidental coincidence results in enhancement of fluorescence.

To gain more insight into the mechanism of the generation of light from the fluorophore-ZnO complex, the photoexcitation processes have been shown in the Figure 5. The two types of transition i.e., n– π * and π – π * exists in the fluorophore. Due to the lower availability of the non-bonding electrons, the π – π * transition is more prominent, which will give rise to the blue emission around 420 nm. In ZnO nanocrystals, some O^{2-} ions can escape from the host lattice, leading to formation of oxygen vacancies. This oxygen vacancy centre can trap an electron, leading to the formation of defect states [29]. There are three energy levels viz. VB, defect states and CB. ZnO nanocrystals first create positive holes in the VB and negative electrons in the CB after photoexcitation. The hole in the VB can be traped at the oxygen vacancy sites. Then, this surface trapped hole tunnels back into the particle to recombine with an electron to form the defect states at the surface of the particle. Then recombination of this centre with an electron in the CB gives rise to emission [30]. Upon photoexcitation of the complex, the π – π * transition of fluorophore gives blue light and the transition between the electron in the CB and hole trapped in the defect states give rise to emission at longer wavelength. The emission intensity of fluorophore bound to ZnO is far larger than that of the isolated molecule. With the fluorophore adsorbed on ZnO the semiconductor is also excited on irradiation. The recombination of the electron in the oxygen vacancies with the hole in the VB results in emission at 421 nm. In addition, emission from the LUMO of the fluorophore adsorbed on ZnO to the CB of ZnO at 421 nm is possible. Due to the additional path opened up for emission the emission intensity is increased.

3.4. Fluorescence switched off by Mn-doped TiO_2 and $BaTiO_3$ nanoparticles

Figure 6 displays the emission of fluorophore at different loading of Mn-doped TiO_2 and $BaTiO_3$ nanoparticles. Addition of these nanoparticles to fluorophore results in fluorescence

switched off. This may be because of electron transfer from LUMO of the fluorophore to CB of nanoparticles. The energy levels presented in Figure 5. The energy gap between the LUMO of the fluorophore to CB of $BaTiO_3$ nanoparticles is 3.2 eV and this energy does not match with that between LUMO and HOMO of the fluorophore. Thus the transfer of electron from LUMO of the fluorophore to CB of $BaTiO_3$ nanoparticles quenches the fluorescence. In Mn-doped TiO_2, TiO_2 is in anatase form [23b], anatase quenches the fluorescence of the fluorophore and this is due to steric reasons [30]. Hence in Mn-doped TiO_2 also inhibition of fluorescence is observed. The apparent association constants (K_{app}) have been obtained [31] from the fluorescence quenching data using the following equation,$1/(F_0 - F) = 1/(F_0 - F') + 1/ K_{app} (F_0 - F')$ [nanoparticles], where F_0 is the fluorescence intensity of the bare fluorophore, F' is the fluorescence intensity of the fluorophore adsorbed on Mn-doped TiO_2 and $BaTiO_3$ nanoparticles and F is the observed fluorescence intensity at different loading of Mn-doped TiO_2 and $BaTiO_3$ nanoparticles. Quenching of fluorescence by nanoparticlulate $BaTiO_3$ in much stronger than that by Mn-doped TiO_2 nanoparticles and the binding constants have been evaluated. The values of apparent association constant (K_{app}) for fluorophore – Mn-doped TiO_2 and fluorophore – $BaTiO_3$ are 4.1×10^5 and 2.8×10^4 M^{-1}, respectively. The number of binding site in the association of the fluorophore with $BaTiO_3$ and Mn-doped TiO_2 nanoparticles have been deduced as 1.01 and 0.89, respectively. This contrasting difference in the binding sites of the core/shell and core nanoparticles show the difference in the binding of the fluorophore with the semiconductor surface. Furthermore the fluorophore binds much stronger with the ZnO than with the core nanomaterials.

3.5. Free-energy change (ΔG_{et}) for electron transfer process

The thermodynamic feasibility of excited state electron transfer reaction has been confirmed by the calculation of free energy change by employing the well known Rehm-Weller expression, $\Delta G_{et} = E^{1/2}_{(ox)} - E^{1/2}_{(red)} - E_s + C$, where, $E^{1/2}_{(ox)}$ is the oxidation potential of fluorophore, $E^{1/2}_{(red)}$ is the reduction potential, that is, the CB potential of semiconductor nanoparticles, E_s is the excited state energy of fluorophore and C is the coulombic term. Since the fluorophore is neutral and the solvent used is polar in nature, the coulombic term in the above expression can be neglected [31]. The values of ΔG_{et} for ZnO, $BaTiO_3$/ZnO and Mn-doped TiO_2/ZnO core/shell nanospheres are calculated as −3.62 eV. The negative value indicates the thermodynamic feasibility of the electron transfer process [32]. The energy of electron transfer from fluorophore to Mn-doped TiO_2/ZnO and $BaTiO_3$/ZnO core/shell and pristine ZnO nanospheres are the same these is because the electron transfer is to the CB of ZnO shell or ZnO nanocrystal. The core Mn-doped TiO_2 and $BaTiO_3$ are completely wrapped by the ZnO shell thereby ruling out the possibility of electron transfer to the Mn-doped TiO_2 core or $BaTiO_3$ core.

3.6. Fluorescence lifetime studies

An alternative way to rationalize the behaviour observed in the present study is by considering the fluorescence lifetime ($\boldsymbol{\tau}$) of fluorophore. Figure 6 displays the fluorescence decay of fluorophore. The decay follows a bi-exponential fit indicating fluorophore is in two excited states - one is likely to be the configuration in which the styryl moiety is coplanar with the imidazole ring and other is one with the styryl ring perpendicular to the imidazole ring. The X-ray crystal structure and theoretical calculation [22] show the perpendicular configuration as most stable. Hence the observed longer lifetime is attributed to the perpendicular configuration of the fluorophore. Evaluation of the radiative (k_r) and non-radiative (k_{nr}) rates show that the

radiative emission is predominant over the non-radiative emission. The radiative and non-radiative decay of the excited state have been obtained using the quantum yields(Φ)and lifetimes(τ). The formulae employed to calculate the radiative (k_r) and non-radiative (k_{nr}) rate constants are, $k_r = \Phi / \tau$; $k_{nr} = (1/\tau) - (\Phi/\tau)$, where $\tau = (k_r + k_{nr})^{-1}$. The k_r and k_{nr} values are displayed in Table 1. Emission of the fluorophore bound to pristine ZnO and core/shell Mn-doped TiO_2/ZnO and $BaTiO_3$/ZnO nanospheres follow single exponential decay whereas the fluorophore attached to Mn-doped TiO_2 and $BaTiO_3$ nanoparticles display biexponential decay. This is because of the nature of binding of the fluorophore with the semiconductor surface. The number of binding sites in the case of pristine ZnO and core/shell Mn-doped TiO_2/ZnO and $BaTiO_3$/ZnO nanospheres is two whereas those with Mn-doped TiO_2 and $BaTiO_3$ nanoparticles are one. Since the fluorophore is bound with two under coordinate surface Zn^{2+} on the surface of the nanocrystal the orientation of the fluorophore is restricted i.e., unlike in the case of free ligand, the ligand bound to ZnO or ZnO shell can take up only one form. As the fluorophore exist in only one form single exponential decay is observed with ZnO and core/shell Mn-doped TiO_2/ZnO and $BaTiO_3$/ZnO nanospheres. In the case of fluorophore bound with Mn-doped TiO_2 and $BaTiO_3$ nanoparticles the single binding site allows the fluorophore to take up two different orientations enabling the biexponential decay.

According to Forster's energy transfer theory, the energy transfer efficiency is related not only to the distance between the acceptor and donor (r_0), but also to the critical energy transfer distance (R_0). That is, $E = R^6_0/(R^6_0 + r^6_0)$, where, R_0 is the critical distance when the transfer efficiency is 50% and $R^6_0 = 8.8 \times 10^{-25} K^2 N^{-4} \varphi J$, where, K^2 is the spatial orientation factor of the dipole, N is the refractive index of the medium, φ is the fluorescence quantum yield of the donor and J is the overlap integral of the fluorescence emission spectrum of the donor and the

absorption spectrum of the acceptor [33]. The value of J can be calculated by using the equation, $J = \int F(\lambda)\varepsilon(\lambda)\lambda^4 d\lambda / F(\lambda)d\lambda$, where, $F(\lambda)$ is the fluorescence intensity of the donor and $\varepsilon(\lambda)$ is molar absorptivity of the acceptor. The evaluated parameters J, E, R_0 and r_0 are listed in Table 1. Obviously, the calculated value of R_0 is in the range of maximal critical distance. This is in accordance with the conditions of Forster's energy transfer theory and suggests that energy transfer occurs between the semiconductor nanoparticles and fluorophore with high probability. The evaluated distance between the fluorophore and the Mn-doped TiO_2/ZnO, $BaTiO_3$/ZnO core/shell and ZnO nanosphere are the same and this supports the ZnO-fluorophore binding in all the cases. The donar-acceptor distance in Mn-doped TiO_2 nanoparticles is lower than that of the others. This also supports the interaction of fluorophore with Mn-doped TiO_2 is different from Mn-doped TiO_2/ZnO core/shell and ZnO nanospheres. Core–shell nanoparticles attract much interest as they have emerged at the frontier of materials chemistry and have different applications like bio-imaging, controlled drug release, targeted drug delivery, cell labelling, tissue engineering, electronics, photoluminescence, catalysis etc., [34] and the knowledge about their interaction with biologically important molecules such as steroids, phenanthrimidazoles may have possible applications in the listed fields.

4. Conclusions

To conclude, Mn-doped TiO_2/ZnO, $BaTiO_3$/ZnO core/shell and ZnO nanospheres switched on the fluorescence of styryl phenanthrimidazole whereas Mn-doped TiO_2 and $BaTiO_3$ nanoparticles switched off the fluorescence. Accidently the wavelength of emission of the fluorophore matches with that of deep level emission of ZnO which results in enhancement of fluorescence, the electron transfer from LUMO to the defect levels of ZnO through the CB of ZnO yields deep level emission. The energy gap between LUMO and CB of $BaTiO_3$ is large and

hence quenching of fluorescence is observed. The anatase phase of Mn-doped TiO_2 quenches the fluorescence of the fluorophore. The contrasting emission behaviour is also a consequence of the nature of binding of the fluorophore with ZnO and the core nanoparticles.

5. Acknowledgments

One of the authors Prof. J. Jayabharathi is thankful to DST [No. SR/S1/IC-73/2010], UGC (F. No. 36-21/2008 (SR), DRDO (NRB-213/MAT/10-11) and CSIR **(**No 3732/NS-EMRII**)** for providing funds to this research study.

References

[1] Y.F. Lin and W.B. Jian, The impact of nanocontact on nanowire based nanoelectronics, Nano Lett. 8 (2008) 3146-3150.

[2] X. D. Wang, C.J. Summers and Z.L. Wang, Large-scale Hexagonal-Patterned Growth of Aligned ZnO Nanorods for Nano-optoelectronics and Nanosensor Arrays, Nano Lett. 4 (2004) 423-426.

[3] X. Wang, J. Song and Z.L. Wang, Nanowire and nanobelt arrays of zinc oxide from synthesis to properties and to novel devices, J. Mater. Chem. 17 (2007) 711-720.

[4] S.C. Pillai, J.M. Kelly, R. Ramesh and D.E. McCormack, Advances in the synthesis of ZnO nanomaterials for varistor devices, J. Mater. Chem. C 1 (2013) 3268-3281.

[5] T. Premkumar, Y.S. Zhou, Y.F. Lu and K. Baskar, Optical and field emission properties of ZnO nanostructures deposited using high&pressure pulsed laser deposition, ACS Appl. Mater. Interfaces. 2 (2010) 2863-2869.

[6] H. Faber, M. Klaumunzer, M. Voigt, D. Galli, B.F. Vieweg, W. Peukert, E. Spiecker and M. Halik, Morphological impact of zinc oxide layers on the device performance in thin-film transistors**,** Nanoscale, 3 (2011) 897-899.

[7] D. Vanmaekelbergh and L.K. van Vugt, ZnO nanowire lasers, Nanoscale, 3 (2011) 2783-2800.

[8] J.A. Anta, E. Guillen and R. Tena-Zaera, ZnO-based dye-sensitized solar cells, J. Phys. Chem. C 116 (2012) 11413-11425.

[9] D. Barreca, D. Bekermann, E. Comini, A. Devi, R.A. Fischer, A. Gasparotto, C. Maccato, G. Sberveglieri and E. Tondello, 1D ZnO nano-assemblies by Plasma-CVD as chemical sensors for flammable and toxic gases, Sens. Actuators B. 149 (2010) 1-7.

[10] B. Faure, G. Salazar-Alvarez, A. Ahniyaz, I. Villaluenga, G. Berriozabal, Y.R. De Miguel and L. Bergstrom, Dispersion and surface functionalization of oxide nanoparticles for transparent photocatalytic and UV-protecting coatings and sunscreens, Sci. Technol. Adv. Mater. 14 (2011) 023001.

[11] J. Hu, Y. Fan, Y. Pei, M. Qiao, K. Fan, X. Zhang and B. Zong, ACS Catal. 3 (2013) 2280-2287.

[12] J. Becker, K.R. Raghupathi, J. St. Pierre, D. Zhao and R.T. Koodali, Tuning of the Crystallite and Particle Sizes of ZnO Nanocrystalline Materials in Solvothermal Synthesis and Their Photocatalytic Activity for Dye Degradation, J. Phys. Chem. C 115 (2011) 13844-13850.

[13] K.R. Raghupathi, R.T. Koodali and A.C. Manna, Size-dependent bacterial growth inhibition and mechanism of antibacterial activity of zinc oxide nanoparticles, Langmuir, 27 (2011) 4020-4028.

[14] M. Wang, N. Chamberland, L. Breau, J.E. Moser, R. H. Baker, B. Marsan, S.M. Zakeeruddin and M. Gratzel, An organic redox electrolyte to rival triiodide/iodide in dye-sensitized solar cells, Nature Chem. 2 (2010) 385-389.

[15] A. Panariti, G. Miserocchi and I. Rivolta, The effect of nanoparticle uptake on cellular behavior: disrupting or enabling functions, Nanotechnol. Sci. Appl. 5 (2012) 87-100.

[16] R. Hariharan, S. Senthilkumar, A. Suganthi and M. Rajarajan, Synthesis and characterization of doxorubicin modified ZnO/PEG nanomaterials and its photodynamic action, J. Photochem. Photobiol. B 116 (2012) 56-65.

[17] K.E. Knowles, M.T. Frederick, D.B. Tice, A.J. Morris-Cohen and E.A. Weiss, Colloidal Quantum Dots: Think Outside the (Particle-in-a-) Box, J. Phys. Chem. Lett. 3 (2012) 18-26.

[18] E.A. Frederick, L.C. Cass, V.A. Amin and E.A. Weiss, A Molecule to Detect and Perturb the Confinement of Charge Carriers in Quantum Dots, Nano Lett. 11 (2011) 5455-5460.

[19] K.E. Knowles, D.B. Tice, E.A. McArthur, G.C. Solomon and E.A. Weiss, Chemical Control of the Photoluminescence of CdSe Quantum Dot-Organic Complexes with a Series of p-Substituted Aniline Ligands, J. Am. Chem. Soc. 132 (2010) 1041-1050.

[20] W.S. Hung, J.T. Lin, C.H. Chien, Y.T. Tao, S.S. Sun and Y.S. Wen, Highly phosphorescent bis-cyclometallated iridium complexes containing benzoimidazole-based ligands, Chem. Mater. 16 (2004) 2480-2488.

[21] M. J. Frisch, G. W. Trucks, H. B. Schlegel, G. E. Scuseria, M. A. Robb, J. R. Cheeseman, J. A. Montgomery, Jr., T. Vreven, K. N. Kudin, J. C. Burant, J. M. Millam, S. S. Iyengar, J. Tomasi, V. Barone, B. Mennucci, M. Cossi, G. Scalmani, N. Rega, G. A. Petersson, H. Nakatsuji, M. Hada, M. Ehara, K. Toyota, R. Fukuda, J. Hasegawa, M. Ishida, T.Nakajima, Y. Honda, O. Kitao, H. Nakai, M. Klene, X. Li, J. E. Knox, H. P. Hratchian, J. B. Cross, C. Adamo, J. Jaramillo, R. Gomperts, R. E. Stratmann, O. Yazyev, A. J. Austin, R. Cammi, C. Pomelli, J. W. Ochterski, P. Y. Ayala, K. Morokuma, G. A. Voth, P. Salvador, J. J. Dannenberg, V. G. Zakrzewski, S. Dapprich, A. D. Daniels, M. C. Strain, O. Farkas, D. K. Malick, A. D. Rabuck, K. Raghavachari, J. B. Foresman, J. V. Ortiz, Q. Cui, A. G. Baboul, S. Clifford, J. Cioslowski, B. B. Stefanov, G. Liu, A. Liashenko, P. Piskorz, I. Komaromi, R. L. Martin, D. J. Fox, T. Keith, M. A. Al-Laham, C. Y. Peng, A. Nanayakkara, M. Challacombe, P. M. W. Gill, B. Johnson, W. Chen, M. W. Wong, C. Gonzalez, J. A. Pople, Gaussian, Inc., Pittsburgh PA. (2003).

[22] V. Thanikachalam, J. Jayabharathi, A. Arunpandiyan and P. Ramanathan, Photophysical properties of the intramolecular excited charge-transfer states of π-expanded styryl phenanthrimidazoles – effect of solvent polarity, RSC adv. 4 (2014) 6790-6806.

[23] (a) C. Karunakaran, P. Vinayagamoorthy and J. Jayabharathi, Optical, electrical, and photocatalytic properties of polyethylene glycol-assisted sol–gel synthesized $BaTiO_3$@ZnO core–shell nanoparticles, Powder Technol. 254 (2014) 480-487; (b) C. Karunakaran, J. Jayabharathi and P. Vinayagamoorthy, Electrical, optical and photocatalytic properties of polyethylene glycol-assisted sol–gel synthesized Mn-doped TiO_2/ZnO core–shell nanoparticles, Superlattice Microst. 64 (2013) 569-580.

[24] H. C. Zeng, Ostwalds ripening: A synthetic approach for hallow nanomaterials, Curr. Nanosci., 3 (2007) 177-181.

[25] (a) J. Jayabharathi, V. Thanikachalam, V. Kalaiarasi and K. Jayamoorthy, Enhancing photoluminescent behavior of 2-(naphthalen-1-yl)-1,4,5-triphenyl-1H-imidazole by ZnO and Bi_2O_3, Spectrochim.Acta Part A. 118 (2014)182-186.

[26] (a) G.Z. Chen, X.Z. Huang, J.G. Xu, Z.B. Wang and Z.Z. Zheng, Method of Fluorescent Analysis (2nd ed.), Science Press, Beijing. (Chapter 4). 126 (1990); (b) A. K. Raychaudhuri and S. K. Pal, Role of Resonance Energy Transfer in Light Harvesting of Zinc Oxide-Based Dye-Sensitized Solar Cells, J. Phys. Chem. C. 114 (2010) 10390-10395; (c) L. Tang, X. Dai, K. Zhong, X. Wen and D. Wu, A Phenylbenzothiazole Derived Fluorescent Sensor for Zn(II) Recognition in Aqueous Solution Through "Turn-On" Excited-State Intramolecular Proton Transfer Emission, J. Fluoresc. 24 (2014) 1487-1493; (d) V. Bhalla, A. Gupta and M. Kumar, A pentacenequinone derivative with aggregation-induced emission enhancement

characteristics for the picogram detection of Fe^{3+} ions in mixed aqueous media, Dalton Trans. 42 (2013) 4464-4469.

[27] A. Kathiravan and R. Renganathan, Photoinduced interaction between colloidal TiO_2 from nanoparticles and calf thymus-DNA, Polyhedron. 28 (2009) 1374-1378.

[28] L. Jing, Y. Qu, B. Wang, S. Li, B. Jiang, L. Yang, W. Fu, H. Fu and J. Sun, Review of photoluminescence performance of nano-sized semiconductor materials and its relationships with photocatalytic activity, Sol. Energ. Mat. Sol. C. 90 (2006) 1773-1787.

[29] L. Zhang, L. Yin, C. Wang, N. Lun, Y. Qi and D. Xiang, Origin of visible photoluminescence of ZnO quantum dots: defect-dependent and size-dependent, J. Phys. Chem. C. 114 (2010) 9651-9658.

[30]C. Karunakaran, J. Jayabharathi, K. Jayamoorthy and K.Brindha Devi, Sensing rutile TiO_2 through fluorescence of imidazole derivative, Sensors and Actuators B. Chem. 168 (2012) 263-270.

[31] S. Jagadeeswari, G. Paramaguru, S. Thennarasu and R. Renganathan, Synthesis, optical and electrochemical properties of carbazole sensitizers and their interaction with TiO_2, J. Mol. Struct. 1060 (2014) 191-196.

[32] G. J. Kavarnos and N. J. Turro, Photosensitization by Reversible Electron Transfer: Theories, Experimental Evidence and Examples, Chem. Rev. 86 (1986) 401-449.

[33] (a) A. Giri, A. Makhal, B. Ghosh, A. K. Raychaudhuri and S. K. Pal, Functionalization of manganite nanoparticles and their interaction with biologically relevant small ligands: Picosecond time-resolved FRET studies, Nanoscale**,** 2 (2010) 2704-2709; (b) A. Makhal, S. Sarkar, T. Bora, S. Baruah, J. Dutta, K. Raychaudhuri and S.K. Pal, Role of Resonance

Energy Transfer in Light Harvesting of Zinc Oxide-Based Dye-Sensitized Solar Cells, J. Phys. Chem. C. 114 (2010) 10390-10395.

[34] R.G. Chaudhurai and S. Paria, Core/shell nanoparticles: classes, properties, synthesis mechanisms, characterization, and applications, Chem. Rev. 112 (2012) 2373-2433.

Figure Captions

Figure 1. HR-SEM images of core/shell (**a**) Mn-doped TiO_2/ZnO and (**b**) $BaTiO_3$/ZnO

Figure 2. The absorption spectra of fluorophore in the absence and presence of core/shell Mn-doped TiO_2/ZnO and $BaTiO_3$/ZnO and pristine ZnO nanospheres and Mn-doped TiO_2 and $BaTiO_3$ nanoparticles dispersed at different loading

Figure 3. (**a**) The emission spectra of fluorophore in the absence and presence of core/shell Mn-doped TiO_2/ZnO and $BaTiO_3$/ZnO and pristine ZnO nanospheres; (**b**) Mn-doped TiO_2 and $BaTiO_3$ nanoparticles at different loading

Figure 4. Stern-Volmer plots

Figure 5. HOMO and LUMO energy levels of fluorophore and CB and VB edges of **(a)** core/shell Mn-doped TiO_2/ZnO, core/shell $BaTiO_3$/ZnO and pristine ZnO nanospheres; **(b)** Mn-doped TiO_2 and $BaTiO_3$ nanoparticles

Figure 6. Lifetime decay of fluorophore (**a**) core/shell Mn-doped TiO_2/ZnO and $BaTiO_3$/ZnO and pristine ZnO nanospheres; (**b**) Mn-doped TiO_2 and $BaTiO_3$ nanoparticles

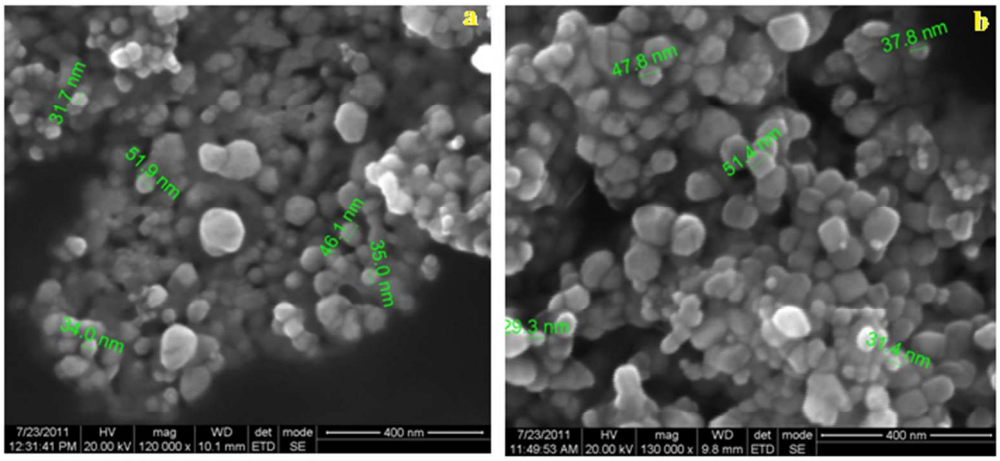

Figure 1

188x96mm (96 x 96 DPI)

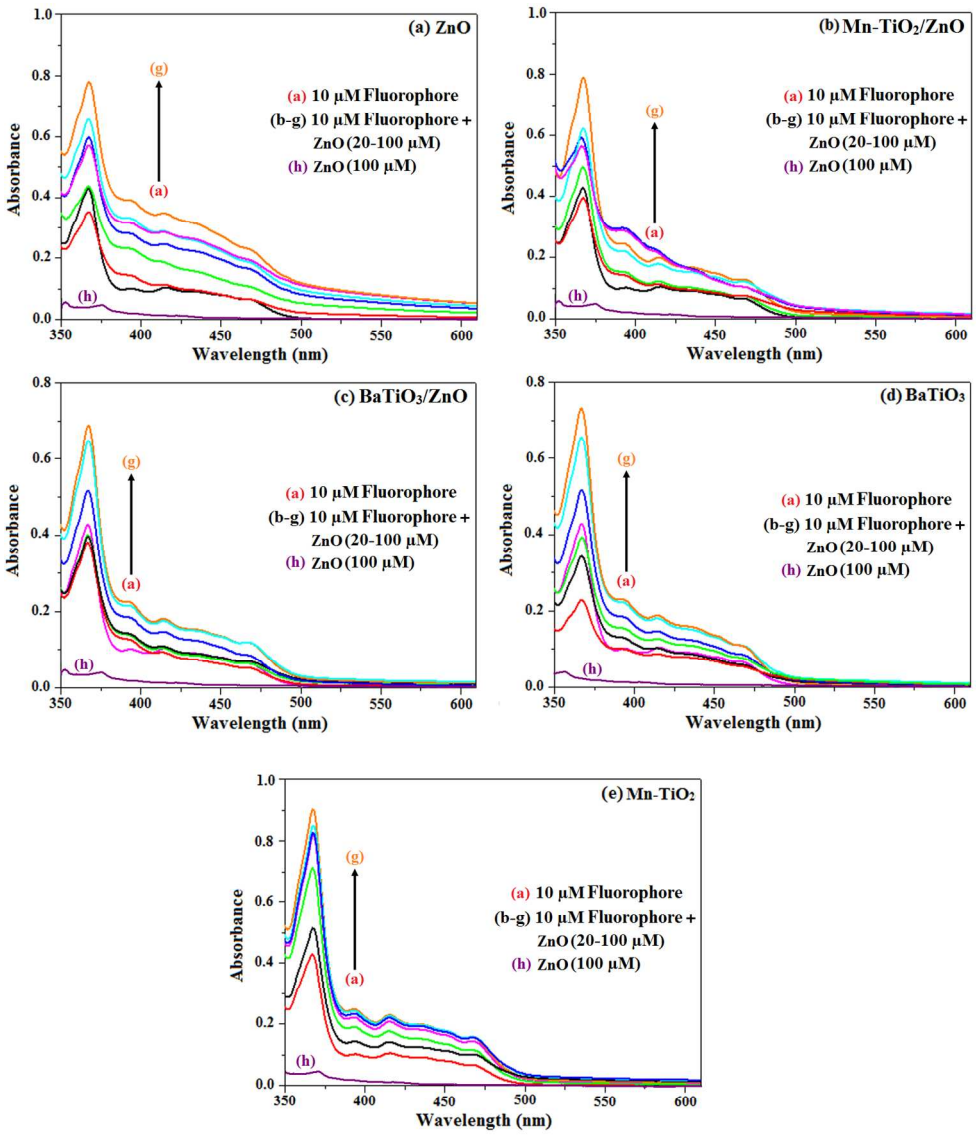

Figure 2

276x337mm (150 x 150 DPI)

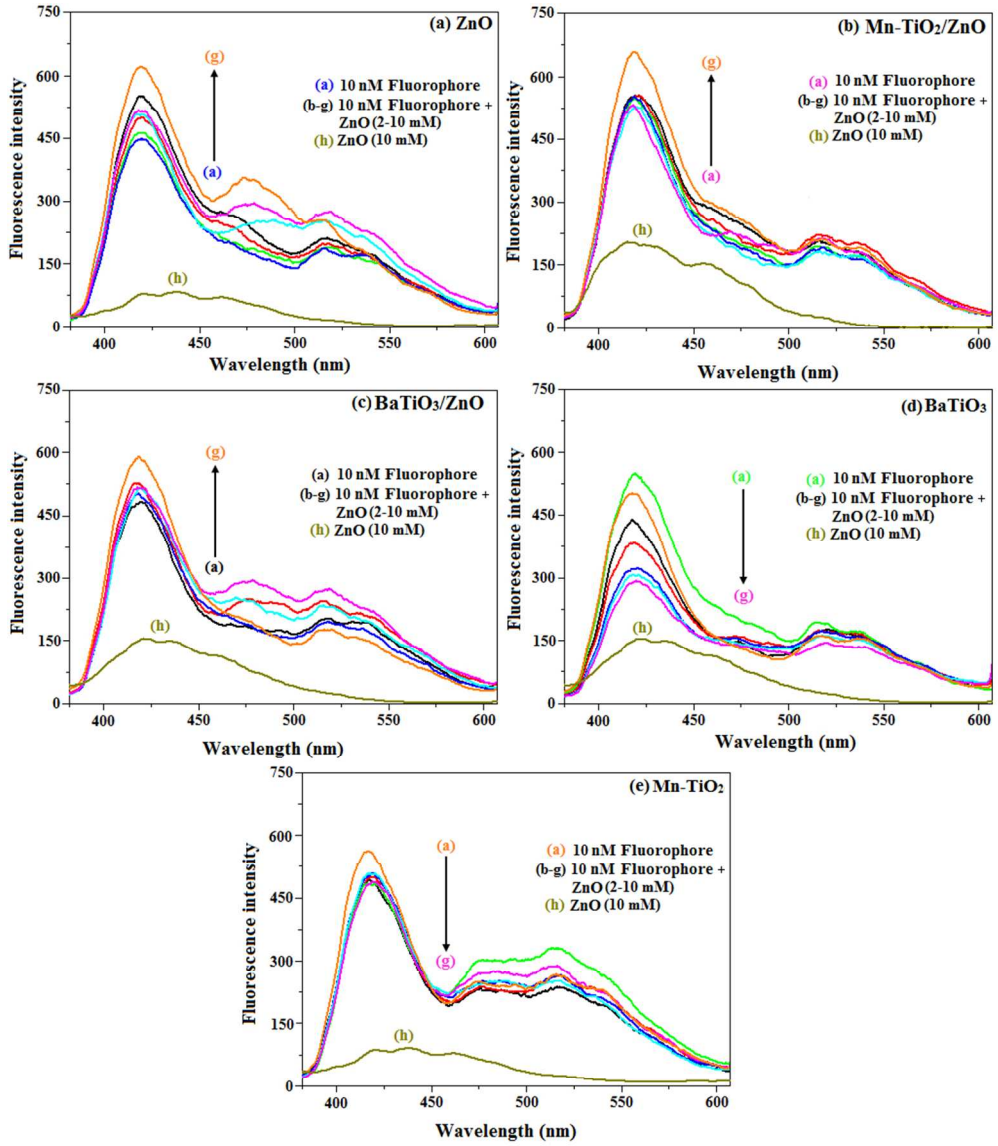

Figure 3

271x320mm (96 x 96 DPI)

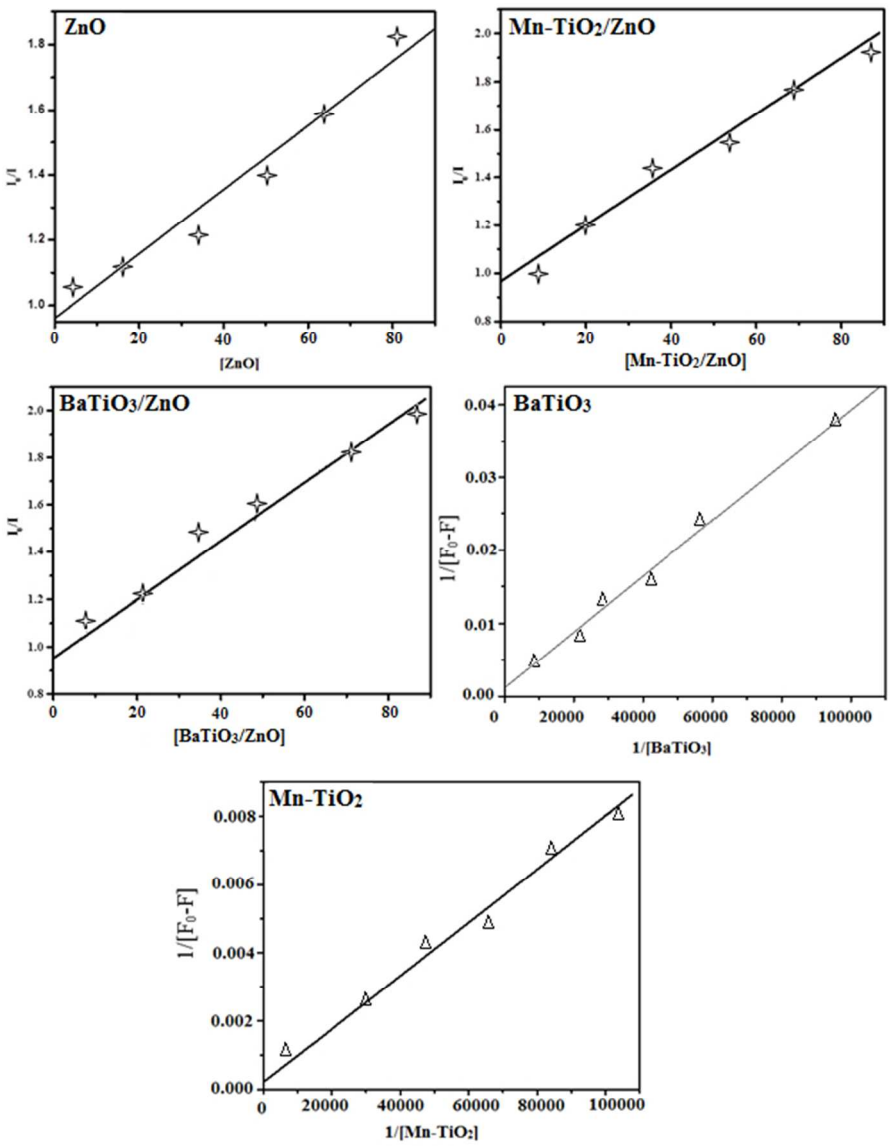

Figure 4

165x222mm (96 x 96 DPI)

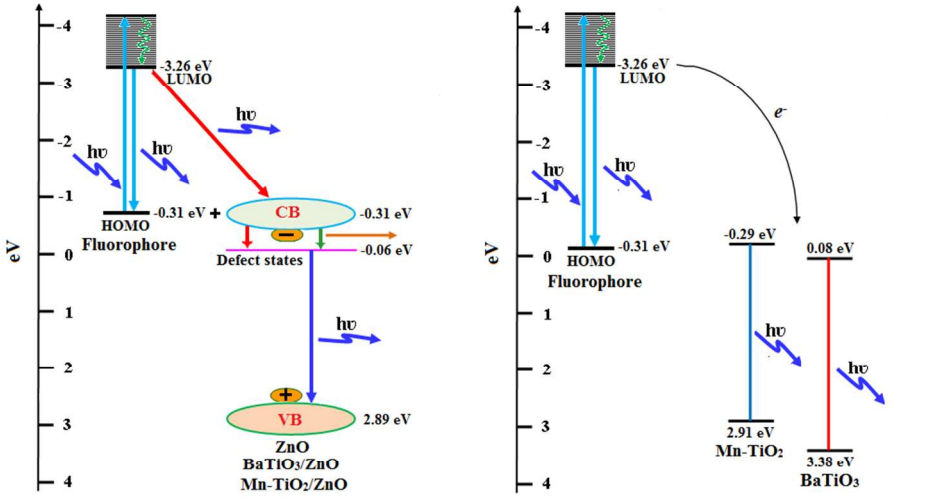

(a) (E)-1-phenyl-2-styryl-1H-phenanthro[9,10-d]imidazoles (PSPI) adsorbed on ZnO (or) $Mn\text{-}TiO_2/ZnO$ (or) $BaTiO_3/ZnO$

(b) (E)-1-phenyl-2-styryl-1H-phenanthro[9,10-d]imidazoles (PSPI) adsorbed $Mn\text{-}TiO_2$ (or) $BaTiO_3$

Figure 5

285x186mm (96 x 96 DPI)

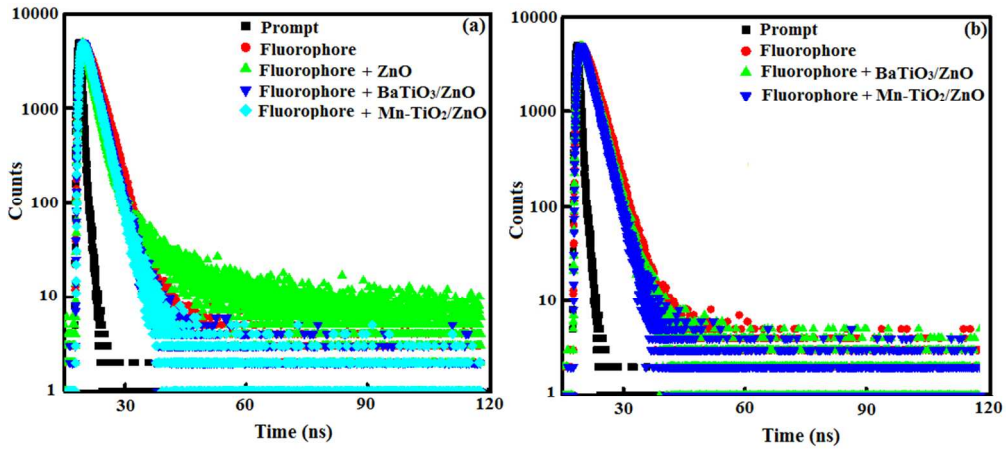

Figure 6

280x137mm (96 x 96 DPI)

Table 1. Lifetime (τ, ns), radiative rate constant (k_r, 10^8 s^{-1}), nonradiative rate constant (k_{nr}, 10^8 s^{-1}) and evaluation of overlap integral (J, $x10^{-11}cm^{-3}$/mol), energy transfer efficiency E, maximal critical distance (R_0, $x10^{-9}$m) and acceptor and donor distance (r_0, nm)

Complex	τ	k_r	k_{nr}	J	E	R_0	r_0
Fluorophore	2.14	5.1	2.3	-	-	-	-
Fluorophore ….ZnO	1.95	2.9	1.2	9.06	0.26	1.48	1.76
Fluorophore ….Mn-TiO_2/ZnO	2.31	3.1	1.3	6.46	0.16	1.40	1.83
Fluorophore ….$BaTiO_3$/ZnO	2.44	2.9	1.2	6.61	0.20	1.40	1.77
Fluorophore …. Mn-TiO_2	2.40	3.0	1.2	1.11	0.19	7.09	0.72
Fluorophore ….$BaTiO_3$	2.59	2.7	1.1	1.10	0.17	2.02	1.46